Analysis of Blood and Bone Marrow Smears using Digital Image Processing Techniques

Heiko Hengen, Susanne Spoor and Madhukar Pandit

All authors:
University of Kaiserslautern, Electrical Engineering and Information Technology,
Chair for Control Systems and Signal Theory,
Erwin Schroedinger Strasse, 67663 Kaiserslautern, Germany

ABSTRACT

In the paper, we deal with the analysis of blood and bone marrow smears. The main aim of this long term project is to obtain a relative frequency histogram of the white blood cells of different lineage and maturity. Especially for clinical application, a proper image normalization and segmentation of the colour images of blood and bone marrow smears are necessary. For the image normalization, two approaches were adopted: a) active image processing for pre acquisition standardization and b) a histogram based method for post acquisition standardization. Both methods are based on the HSI (Hue Saturation Intensity) Transform. We have developed a robust method for the declustering of the inevitable clusters of white blood cells based on a thresholded distance transform and an extended region growing algorithm that in contrast to active contours does not need any parameterization. For a successful classification, medical morphologic features are translated into feature extraction operators: the mesh structure of the cells' nucleus is analyzed using watershed transform and Gabor features, the shape of cell and nucleus is analyzed using a set of rotational invariant contour based features. The colour and granularity of the cytoplasm yield further features for classification. Current work is focused on classification using the presented features.

Keywords: Medical Image Processing, Declustering, Blood and Bone Marrow Analysis, Higher Segmentation Methods, Feature Extraction

1. INTRODUCTION

1.1. The Project and its Goals

The aim of the presented project is to build up an automatic classification system for panoptically (May/Gruenwald/-Giemsa)-stained blood and bone marrow slides. The analysis of blood slides including counting the cells of different lineage and maturity level is a powerful diagnostic tool for the detection of leukemia. Generally speaking, leukemic patients have immature white blood cells in their peripheral blood, which are practically functionless. Depending on the type of leukemia one observes cells from different lineages and maturity levels.

However, there are marginal cases in which only very few cells of a certain type can be found. Non automated processing of such cases is a strenuous task as every single cell has to be classified properly. Next to the leukemic diseases where the white blood cells are immature, there are also cases (e.g. hairy cell leukemia) where one can directly make out typical deformations of the cells.

Whereas systems for the analysis of stained blood cells (either using flow cytometric methods or panoptically stained blood slides) that yield a pre-classification are commercially available, the analysis of bone marrow smears is much more difficult. In order to classify the levels of maturity of the different types of white blood cells (one methodology to determine the type of leukemia), it is necessary to obtain information about the cells in the bone marrow.

Further author information: (Send correspondence to Heiko Hengen)
E-mail: hengen@eit.uni-kl.de, Telephone: ++49 (0) 631 205-2091
Erwin Schroedinger Strasse, 67663 Kaiserslautern, Germany

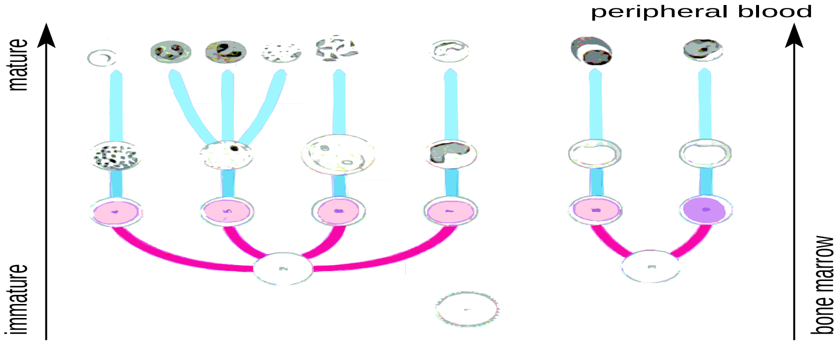

Figure 1. Hematopoiesis; starting with an omnipotent stem cell (1), first pluripotent hematopoietic stem cells (2) and lymphopoietic stem cells (3) develop, which breed the committed stem cells of the Myelopoiesis (4-7) (Erythro-, Granluocyto-, Thrombo-, Monocytopoiesis) and the lymphocytic precursors (8,9). From these stem cells, precursors and finally mature cells develop in bone marrow before they enter the peripheral blood.

1.2. Specific Tasks and Problems

In order to achieve reliable results, the image acquisition has to be standardized in order to yield reproducible results in later classification stages. Concerning standardization, two methods were investigated: a) a priori standardization (during image acquisition) and b) a posteriori standardization (after image acquisition).
Although one obtains suitably standardized input material using one of the two ways, one still has to segment the image, i.e. obtain disjunctive segments for the different cells and their parts (nucleus, cytoplasm) respectively. In the case of peripheral blood, the cells are more or less isolated whereas in the case of bone marrow the cells are extremely clustered. Resolving these clusters is one of the most important steps in the process of analysis. After a successful segmentation including the resolution of the cell clusters, one has to extract features, i.e. compress the information contained in the image segments into a small set of numbers which are later used in order to determine the cell type. As the determination of cell type implies that lineage and maturity level have to be determined, the number of classes is extremely high. Taking also the mutilated cells (e.g. hairy cells) into account, the number of different classes attains around 30. A hierarchical classification using very concise combined features (e.g. combination of texture and colour) that yield simple distinctions are presently elaborated. Using such features a hierarchical rather than a one-step classification is envisaged. This is the current focus.

2. IMAGE ACQUISITION AND STANDARDIZATION

As pointed out above, the image material acquired has to be standardized. This is necessary due to variations in the staining process of the slides and also due to slight irreproducibilities especially concerning the thickness of bone marrow smears.

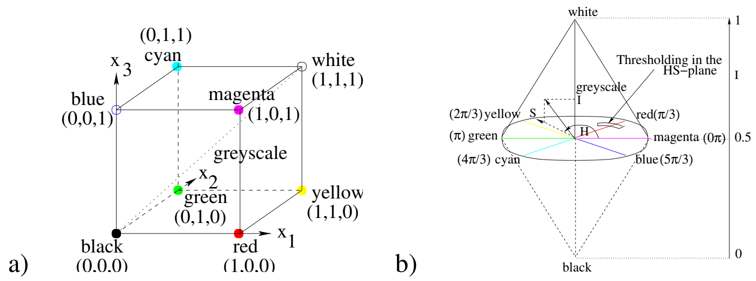

Figure 2. a) RGB colour model, b) HSI colour model with rotated base angle to avoid $0°/360°$ problem in the interesting range of hues

In the following, a priori and a posteriori standardization will be elucidated. The a priori standardization is based on a HSI transformed image of the slide. The microscope is in this case equipped with a video camera. Checking the intensity and

saturation of a piece of image background yields a parameter indicating whether illumination is intense enough and can be either fed back to the automated setup or to the examiner who acquires the images. The a posteriori standardization procedure is not as straightforward but had to be adopted ultimately because the video signals led to colour noise and other disturbances that made texture processing nearly impossible.
The a posteriori method is well suited to a setup using a digital camera. The digital camera used provides a very high resolution and negligible noise effects. The high colour resolution allows a practically lossless standardization based on the intensity histogram of the image as will be shown in the following paragraph. Without a priori standardization, each blood or bone marrow smear is taken at different levels of brightness owing to the preferences of the operator and resulting in yellowish or brownish background and a consequential discolouration of contained cells. Hence a linear transformation of the background to a standardized value results in normalization of the important information carriers, the white blood cells. Thus a histogram transform with properly selected range is proposed. Background information can easily be extracted by using an intensity histogram of the smear as depicted in Fig. 4, containing the intensity histograms of Fig. 3a) and b). Residual variance in colour of cells is resulting from slightly different staining of blood smear during preparation of excerpt.

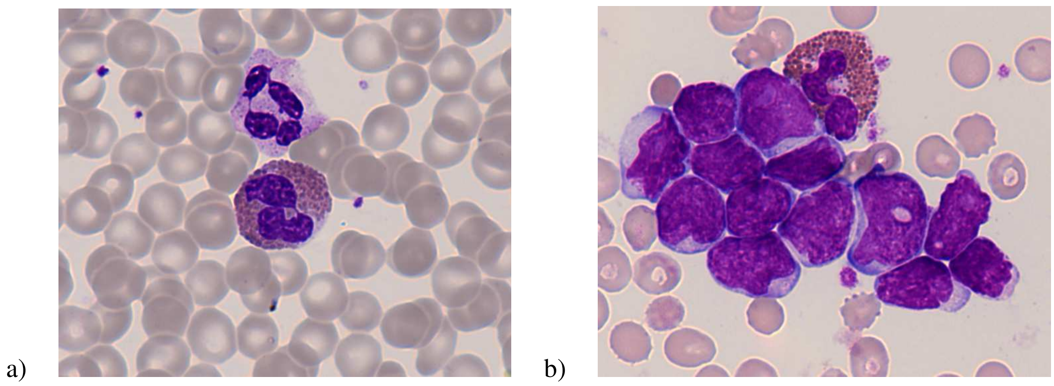

Figure 3: a) non-standardized blood smear image, b) non-standardized bone marrow image

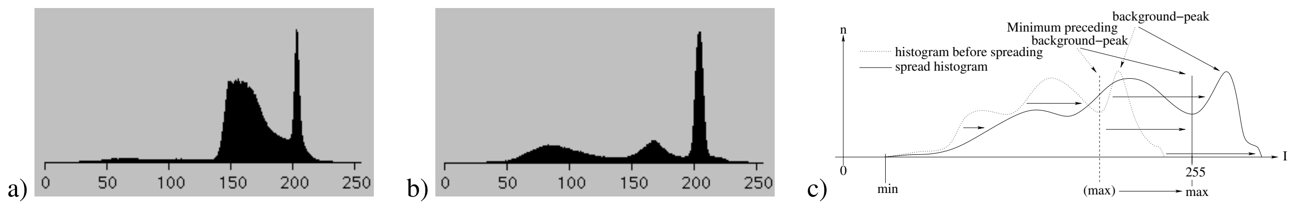

Figure 4. a) Intensity-Histogram of blood smear image, b) Intensity-Histogram of bone marrow image, both of Fig. 3, c) schematic of spreading of Intensity-Histogram for normalization of smear images

Incidentally the intensity histogram obtained from HSI-Transform is in fact suited to the elimination of background effects. The intensity $\mathbf{I}(x, y)$ can be calculated for each pixel from the image data as follows

$$\mathbf{I}(x,y) = \frac{\mathbf{R}(x,y) + \mathbf{G}(x,y) + \mathbf{B}(x,y)}{3}, \tag{1}$$

with $\mathbf{R}(x, y)$, $\mathbf{G}(x, y)$ and $\mathbf{B}(x, y)$ being the red, green and blue matrices of the RGB-image. The resulting Intensity-Histogram features information only in a certain range owing to the specialized content of the images. The first pronounced peak on the high valued side of the histogram depicts the background. A normalization can be achieved by spreading the histogram in such a way that the minimal value (min) is retained while the minimum preceding the background-peak (max) is spread to the maximum, see Fig. 4c) and Eqn. 2. Values exceeding the maximal value of the histogram are set to the maximum value (255), in effect cutting of the histogram and thus eliminating the background completely i.e. assigning it maximal intensity, while normalizing all non-background pixels. $\mathbf{I}_{\text{new}(x,y)}$ being the new $\mathbf{I}(x,y)-$value after the spreading of the histogram. With min and max defined above and in Fig. 4, the new intensity $\mathbf{I}_{\text{new}(x,y)}$ is

$$\mathbf{I}_{\text{new}}(x,y) = \frac{\mathbf{I}(x,y) - \min}{\max - \min} \cdot (255 - \min) + \min\,. \tag{2}$$

Retrieval of RGB-Image is done by assigning percentage shares of the intensity value where values larger than the maximal value are set to the maximum value. For computational robustness, a binomial smoothing of the histogram is performed. This has no bearing on the reconstruction of the image since it is not utilized in the calculation of the new $\mathbf{R}(x,y)-$, $\mathbf{G}(x,y)-$ and $\mathbf{B}(x,y)-$values, there the originally computed intensity is used. The apprehension that this method could destroy signal information can be overcome by analyzing the thresholded image, as depicted in Fig. 5 in which the threshold is set to $\max$ i.e. the background-peak preceding minimum. All white areas are designated background and will be set to maximum intensity. The areas within white blood cells or Erythrocytes labeled as background are only those in which one can see through the cell and thus get background information only. Fig. 6 shows the normalized images of Fig. 3.

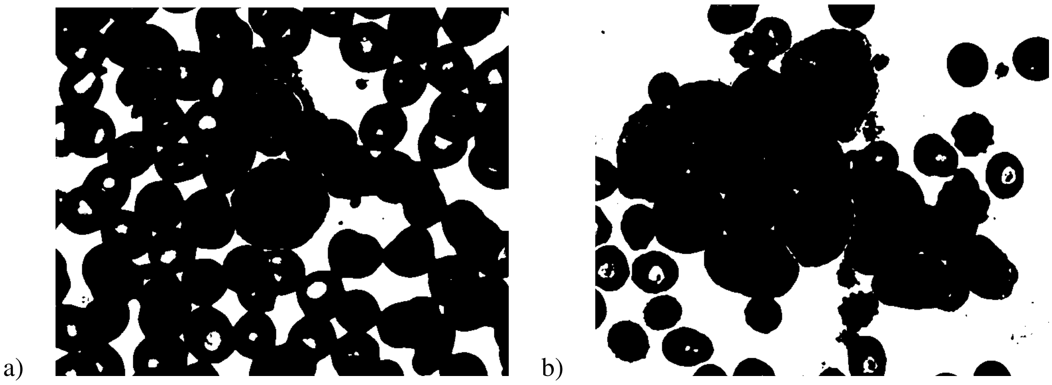

Figure 5. a) Thresholded intensity image of blood smear image, b) thresholded intensity image of bone marrow image, both of Fig. 3 with background-peak preceding minimum as threshold value

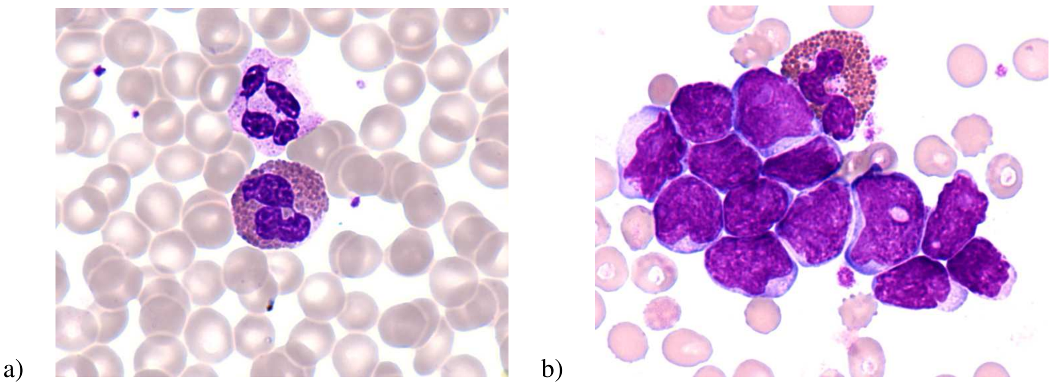

Figure 6: a) Normalized blood smear image, b) normalized bone marrow image, both of Fig. 3

3. PRE-SEGMENTATION

In order to be able to extract features from the white blood cells and to be able to attempt classification, the cells in question have to be available individually. Thus pre-segmentation is necessary to detect white blood cells in smears and to split up clusters of cells into individual cells. Detection of cells can be accomplished by adaptive thresholding in the

HS-plane of the HSI transformed image, see Eqns. 3 and 4. Here the base angle of the HSI-Transform is rotated in order to avoid the $0°/360°$ problem in the interesting range of hues as depicted in Fig. 2. By utilizing an adaptive thresholding method as mentioned above, single white blood cells and clusters can be isolated from the rest of the image. Adaptive thresholding in the hue/saturation-plane is given as

$$\mathbf{Y}(\mathrm{x},\mathrm{y}) \quad = \quad \{\mathrm{Hue}(h_1 < \mathbf{I}(x,y) < h_2) \wedge \mathrm{Sat}(\mathbf{I}(x,y) > s(\mathrm{Sat}(\mathbf{I}(x,y)))\}, \tag{3}$$

where $\mathbf{Y}(x,y)$ is the output image and $\mathbf{I}(x,y)$ the input image while s, h_1 and h_2 denote the thresholds for hue and saturation. Hue$(\ldots)$ and Sat$(\ldots)$ refer to the hue and saturation matrices of the images as a result of the rotated HSI-transform. $s(\mathrm{Sat}(\mathbf{I}(x,y)))$ is given by the adaptive determination of the threshold given in the next Eqn. 4:

$$s(\mathrm{Sat}(\mathbf{I}(x,y)) = \frac{c}{\frac{1}{NM}\sum_{i=0}^{N-1}\sum_{j=0}^{M-1}\mathrm{Sat}(\mathbf{U}(x,y))} \tag{4}$$

Here c is an arbitrary constant, $\mathbf{U}(x,y)$ is the background of the image; the numerical difference in Hue between background and all kinds of foreground objects is high enough, with respect to the metric $\rho(\mathrm{Hue}(\mathbf{F}(x,y)), \mathrm{Hue}(\mathbf{U}(x,y)) > \epsilon$ with $\epsilon \in R$ large enough, $\mathbf{F}(x,y)$ denotes the foreground. In the case of normalized image material as discussed in the previous section, extraction of cells becomes easier owing to the fact that the possible hues are not spread as widely. If the range of nucleus hues and cytoplasm hues is limited on both sides, a specialized posterization can be presented, where not only correct masks for the cells are generated, but also masks for the nucleus. One feasible method of posterization consists of lowpass filtering (binomial filter), followed by quantization of the HS-plane and unification of the colour structure. Thus proper cell and nucleus masks can be generated.
However, even if cytoplasm and nucleus can be separated from background and other cells such as red blood cells, the problem persists that clusters of white blood cells have to be separated into individual cells to ensure a correct calculation of various features. Especially in bone marrow smears large clusters of cells exist which have to be declustered prior to feature extraction. A viable method for declustering is discussed in the next chapter.

4. DECLUSTERING

Finding the cells' boundaries can be based on two classes of algorithms[1]: *Region growing* and *Active contour models*. Both methods need proper initial areas in order to converge to the cells' true boundaries. A morphological algorithm has been selected as the method of choice and will thus be briefly explained. It uses a fast distance-transform after determination of the cluster mask. A distance-transform yields for every pixel in the transform's input image $\mathbf{I}(x,y)$ the minimal distance to the boundary of the object it is lying in (see Fig. 7a)):

$$\mathbf{Y}(x,y) = \{\min_{\forall k} \parallel (x,y) - \boldsymbol{\eta}(x_k,y_k) \parallel)\} \tag{5}$$

with the result of the distance-transform $\mathbf{Y}(x,y)$, the coordinate of every pixel $\mathbf{x} = (x,y)$ in a uniform area $(x,y) \in \mathbf{A}$. $\boldsymbol{\eta}(x_k,y_k)$ is the surrounding curve of the area. The distance transform can be approximated using a 3×3 structuring element in an iterative algorithm (see Fig. 8). The area $\mathbf{A}$ (e.g. a cell cluster) which is obtained as a two-level grey-image is initialized such that pixels $\mathbf{x} \in \mathbf{A}$ are assigned the value 1, background pixels are set to zero; then the structuring element given in Fig. 8 is moved over the whole image $\mathbf{I}(x,y)$. If all elements in the image below the structuring element take values $\mathbf{i}(x,y) \geq a$ (with $a = 1$ in the first step) then the point below the center of the structuring element is incremented (on the same image). Finally, we first increment a and repeat the process.[1]

The distance-transformed image is then thresholded (see Fig. 8).

The region growing algorithm must be controlled by a condition preventing regions from growing into each other (e.g. the regions given in Fig. 9 would grow together without such a condition). To ensure that the region growing stops at the boundary of the cell, we first label the thresholded distance-transform image and label the cluster and background: the area of the clustered object is labeled with a value ξ, the background is labeled 0. For the initial areas $\mathbf{A}_i^0$ we obtain (the subscript denotes the label-index of the area, the superscript gives the iteration step), $\mathbf{V}(x,y)$ is the labeled thresholded

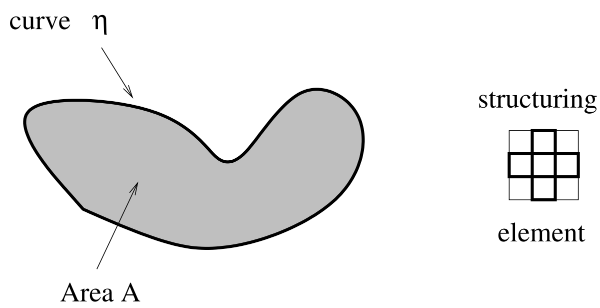

Figure 7: A fast algorithm for distance transform

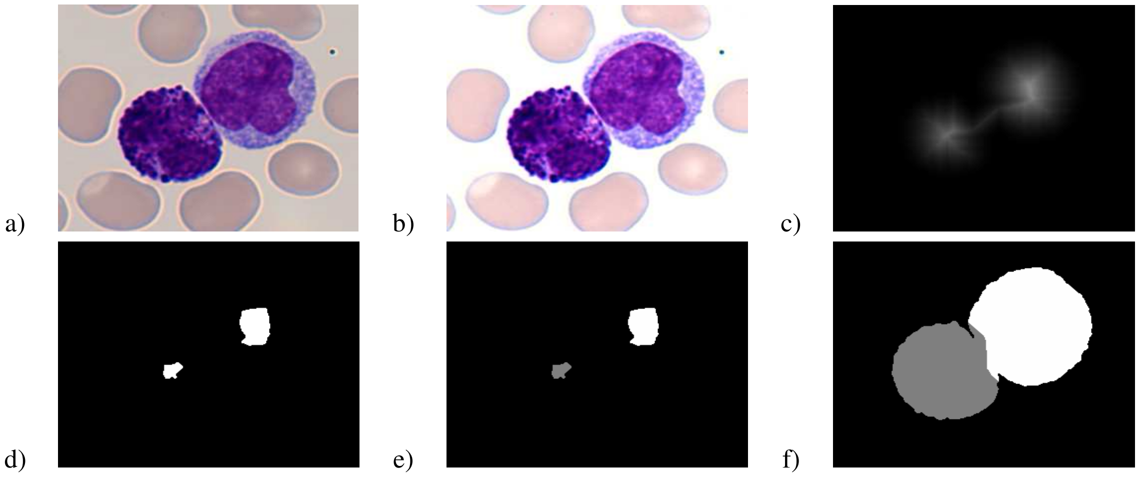

Figure 8. a) Two clustered cells, b) normalized image c) distance transform, d) threshold over distance transform, e) labeled threshold, f) labeled mask of cells

distance-transformed image (see Fig. 8e) and Fig. 9) which consists of regions denoted by the labels i. $\mathbf{X}(x, y)$ is the pre-segmented image:

$$\mathbf{A}_i^0(x, y) = (\mathbf{V}(x, y)|\mathbf{V}(x, y) = i) \tag{6}$$

$$\mathbf{A}_i^{k+1}(x, y) = (\mathbf{A}_i^k \oplus \mathbf{S}) \wedge [(\mathbf{X}^k(x, y) = \xi) \vee (\mathbf{X}^k(x, y) = i)] \tag{7}$$

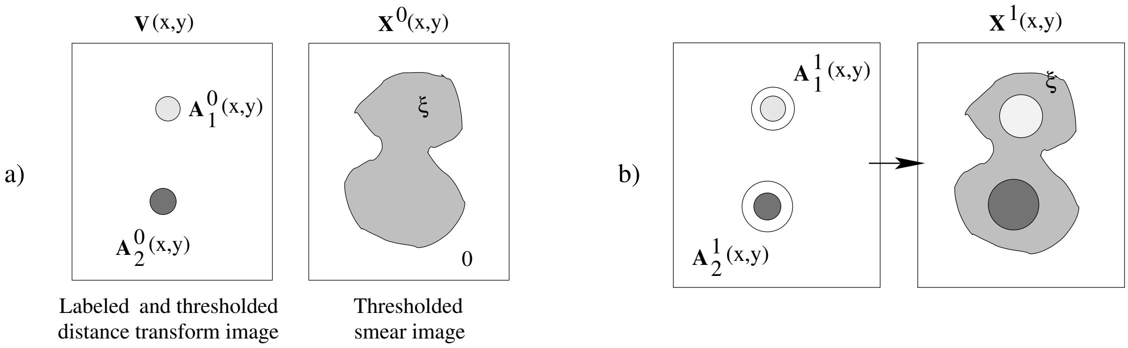

Figure 9: a) Input preparation for the declustering algorithm, b) The first iteration of the declustering algorithm

The dilation $(\mathbf{A}_i^k \oplus \mathbf{S})$ is performed w.r.t the areas labeled i. The iteration is stopped if the areas $\mathbf{A}_i^k$ comprise the whole cluster. The overlapping viz. $(\mathbf{A}_i^k \cap \mathbf{A}_j^k) \neq \emptyset, \; j \neq i$ of the areas is avoided using an extended condition for growing (see

Eqn. (7)) and by introducing results which were already obtained into the source-image $\mathbf{X}(x, y)$ as follows:

$$\mathbf{X}^{k+1}(x,y) \quad = \quad \bigvee_{i=1}^{N} [(\mathbf{X}^k(x,y)|\mathbf{A}_i^{k+1}(x,y) = 0) \vee (\mathbf{A}_i^{k+1}(x,y)|\mathbf{A}_i^{k+1}(x,y) > 0)] \tag{8}$$

The i-th region comprises the whole cell, if $\sum_{i=0}^{M} \left[\text{Pixels}(\mathbf{A}_i^{k+1})\right] - \text{Pixels}(\mathbf{X}(x,y) > 0) = 0$, with Pixels the pixel counting

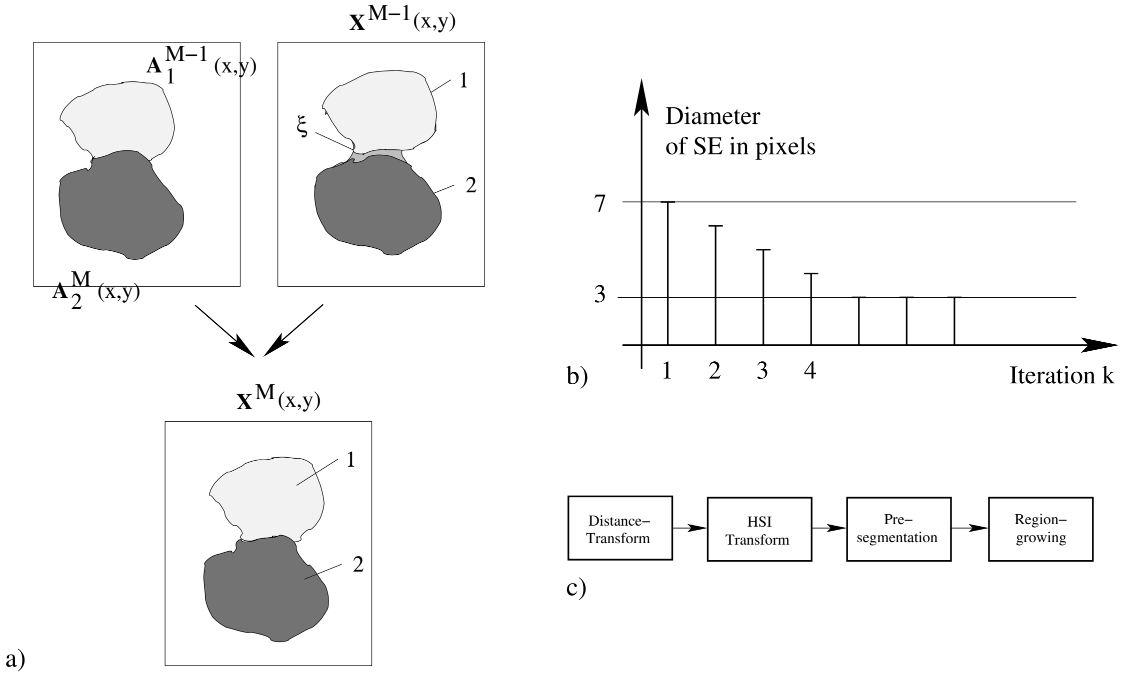

Figure 10. a) The last iteration of the declustering algorithm, b) adaptation of the diameter of the structuring element, c) resulting strategy

operator. As the growing speed of the previously described algorithm is not dependent on the initial contour and the initial area is given by the thresholded distance transform, this method provides a fast - and due to the initialization - yet precise solution for declustering cells.
The described algorithm can be speeded up by varying the size of the structuring element: from iteration to iteration the diameter is decreased (see Fig. 10b)). In order to ensure a Minimum of Artifacts, the selection of a suitable initial diameter of the structuring element has to be selected. A result of the presented declustering algorithm is shown in Fig. 11.

5. FEATURE EXTRACTION

At present, features for cell classification are being developed. This is the crucial step in the whole project. First of all, features, described by physicians are translated into image processing algorithms. Some examples of these features which have already been implemented will be given in the following sections.
While some features such as geometric features which include circumference, thickness, moments and relations, or colour features which include mean and standard deviations, or texture features, some of which are energy, entropy, correlation and homogeneity, are easily calculable, they do not give satisfactory features for the distinction of different cell classes.
One important feature is the number of segments of the nucleus. It is obtained by isolating first the mask of the nucleus itself using colour space methods or pixel classification. Then the mask is subjected to a distance transform which is in turn

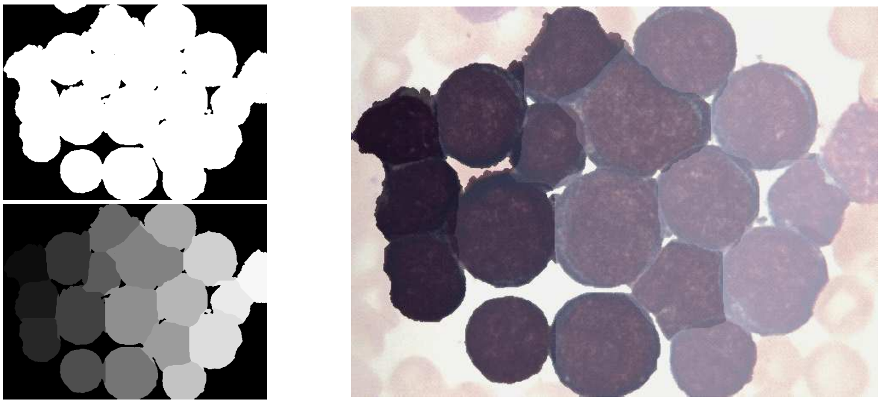

Figure 11. Results - Top left: Mask image of cell cluster obtained by pre-segmentation, Bottom left: mask after declustering process. Right: Overlay of region image and initial colour image of cells

a) 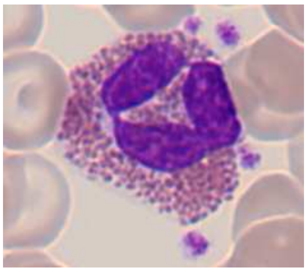 b) 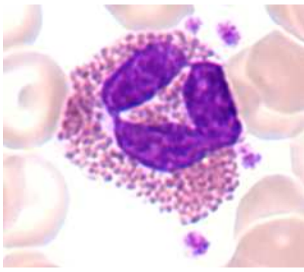 c) 

d) 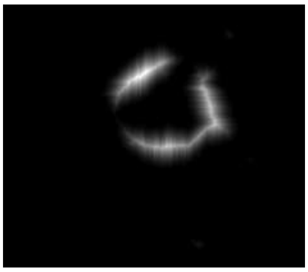 e) 

Figure 12. Detection of number of segments of nucleus: a) original image, eosinophil Granulocyte with segmented nucleus, smear polluted by bursted stained cell b) normalized image, c) mask of nucleus, d) distance transform of mask, e) resulting number of segments

thresholded as depicted in Fig. 12. The resulting number of areas is counted and thus the number of segments is discerned.

Another important feature is the eccentricity $\mathcal{E}$ of the nucleus which can be calculated using the euclidian norm of the difference of the centers of gravity of the nucleus and the whole cell which is comprised of the nucleus and the cytoplasm, with x and y the coordinates of the center of gravity, see Eqn. 9.

$$\mathcal{E} = \sqrt{(x_{\text{cell}} - x_{\text{cyto}})^2 + (y_{\text{cell}} - y_{\text{cyto}})^2} \tag{9}$$

Colour image processing methods are applied in order to exploit significant colour characteristics of the white blood cells that can be used as an additional aid for classification. For example the eosinophilic Granulocytes, basophilic Granulocytes and neutrophilic Granulocytes can be distinguished much easier in colour images than in grey scale. The average colours, standard deviation and mean can be calculated for cytoplasm and nucleus and used as features. In addition to that, a combination of colour and texture based features improves correct classification.

5.1. TEXTURE BASED FEATURES - WATERSHED

One feature which is frequently used by physicians for cell classification is the texture of the nucleus and the texture of the cytoplasm. The texture of the nucleus is often described as a mesh-like structure, the mesh size being an indicator for cell type or maturity level. One possibility is making the texture prominent using morphological transforms and analyzing the number of entries in the Hough-parameter space: fine mesh grids have a higher number of maxima in the parameter space than coarser grids. The method which will be recessed in the following paragraph concerns using a watershed transform[2] for analysis and distinction of the nuclei of different cell types. The algorithm can be applied to cytoplasm accordingly.
The basic idea of the watershed transform is to visualize a digital grey scale image as a landscape, where the altitude of any given coordinate is given by the grey level of the pixel at that point. The lower the grey value, the lower the altitude. A drop of water falling on the surface of this landscape follows the path of steepest descent until it reaches a local minimum. The set of all pixels for which a drop of water will end up in the same minimum is called a catchment basin, the pixels which form the boundaries of those basins are called watershed lines, since it is not possible to predict which way the fictional drop of water will take.
The intuitive approach to the watershed transform is watershed by immersion as depicted in Fig. 13. A grey scale image is visualized as the surface of a landscape where holes have been drilled into all minima, see Fig. 13a). Is the surface immersed in water, the hole in the lowest minimum lets water leak into the catchment basin as shown in Fig. 13b). Is the landscape further submerged, the water of different catchment basins threatens to merge. At that point the watershed lines are raised to prevent such an overflow.

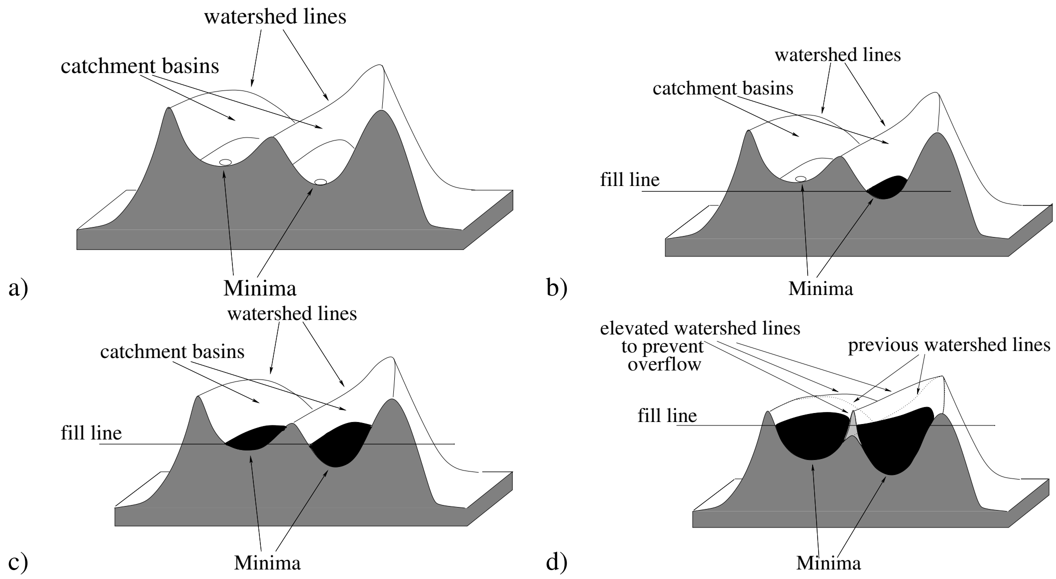

Figure 13. Watershed by immersion: a) landscape before filling b) filling lowest basin, c) filling level increased, d) increased filling level with elevated watershed lines to prevent overflow from one basin to another

This principal procedure can be directly translated into an algorithm evaluating the mesh structures in cells. If a digital grey scale image **I** of dimension $n = 2$ is viewed as a function $f : D \to N$, where the domain of the image is given by $D \subseteq Z^2$ while $h = f(p)$ denotes the grey value of a pixel $p \in D$, a *path* P of length l between two pixels p and p' can be defined by an $(l+1)$-tuple $(p_0, p_1, p_2, ..., p_{l-1}, p_l)$ with $p_0 = p$ and $p_l = p'$ such that $\forall i \in [0, l] : (p_i, p_{i+1}) \in \mathbf{G}$. **G** denotes the underlying grid of the digital image while $h_{\min}$ is the minimum value of f and $h_{\max}$ the maximum value. A minimum M of **I** of the highth h can be defined as an arbitrary area of pixels of grey value h from which no pixel of lower value h', $h' < h$, can be reached without coming across larger values h'' than h, $h'' > h$, as given by the following equations.

$$\forall p \in M, \forall p'' \notin M \quad \text{with} \quad \mathbf{I}(p'') \leq \mathbf{I}(p), \quad \forall P = (p_0, p_1, ..., p_i, ..., p_{l-1}, p_l)$$

Cell-Type	Meshstructure	v	Number of Regions
Promyelocyte	fine mesh	0.79567	124
Myeloblast	fine mesh	0.777037	165
Myeloblast	fine mesh	0.779708	98
Myelocyte	medium coare	1	1
Lymphocyte	coarsely mottled	0.999747	2
Monocyte	coarsely netted	0.999556	2

Table 1: Watershed results in H-domain for different cell-types with different mesh structures

$$\text{with} \quad p_0 = p, \quad p_l = p' \quad \text{and} \quad \exists i \in [1, l] \text{with} \quad \mathbf{I}(p_i) > \mathbf{I}(p_0) \tag{10}$$

By defining a recursion with grey value h increasing from $h_{\min}$ to $h_{\max}$, catchment basins appurtenant with the minima of f are successively expanded. B_h denotes the union of the set of basins computed at level h. A grey value of $h+1$ of the threshold set T_{h+1} can either be a new minimum or an extension of a basin in B_h. In the latter case results in an update of B_{h+1}. min_h constitutes the pool of all regional minima at grey level h.

$$T_h(\mathbf{I}) = \{p \in D_{\mathbf{I}} \mid \mathbf{I}(p) \leq h\}, \;\; B_{h_{\min}}\{p \in D \mid f(p) = h_{\min}\} = T_{h_{\min}} \tag{11}$$

$$B_{h+1} = \mathsf{min}_{h+1} \cup \Phi\{\mathbf{I}, Z\}, \quad Z \in T_{h+1}(B_h), \quad\quad h \in [h_{\min}, h_{\max}] \tag{12}$$

The watershed lines $\mathcal{W}(f)$ of grey scale image $\mathbf{I}$ are the complement of $B_{h_{\max}}$ in D: $\mathcal{W}(f) = D \backslash B_{h_{\max}}$.

Fig. 14 gives the watershed transform of a Myeloblast which is described by physicians as having a fine-mesh structure inside the nucleus and the watershed transform of a Monocyte, the nucleus of which is described as being coarsely meshed. The finer the mesh, the more regions will be found by the watershed transform.

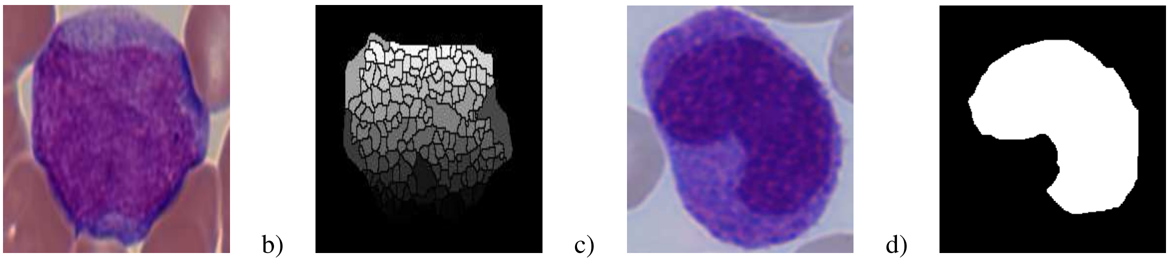
a) b) c) d)

Figure 14. Watershed results for nuclei: a) original Myeloblast image (fine mesh), b) resulting watershed image, 165 regions, c) original Monocyte image (coarse mesh), d) resulting watershed image, one region

$$v = \frac{\text{number of pixels not mesh}}{\text{number of nucleus pixel}} \tag{13}$$

If the area of the nucleus which is not covered by the mesh grid is divided by the total area of the nucleus both in the H domain, a revealing figure is gained for describing the mesh structure. A value of $v < 0.8$ for Eqn. 13 on a scale of 0 to 1 identifies fine-meshed nuclei, all other mesh structures result in values $v > 0.99$ as can be seen in Tab. 1. In Tab. 1 the results of the Watershed are given as applied to the H-domain of the HSI-transform for different cell-types with different mesh structures.

As colour and number of granula encountered in the cytoplasm also yield information about the cell type the same method can be applied along with Haralick-features or wavelet based moments.[3]

6. CLASSIFICATION

The features for cell classification in the previous section form a very small subset of all possible features. For a promising cell classification, one has to make out the most significant features from the cell's image. Two basic ways of cell-classification are possible: a) feature extraction and translation of the features given by physicians into mathematical formulas and b) consideration of every pixel as a feature. Whereas the strategy according to (a) leads to the application of known classification methods (e.g. Gaussian-Bayesian Classifier), (b) implies the usage of a neural network with (rotational invariant) matrix input; such a classifier is trained using all types of white blood cells with no specific features. Here every pixel is a feature and the interrelations between pixels are automatically evaluated in the hidden layers of the network. Currently the features which are implemented are checked for their significance using genetic algorithms in order to provide a smaller feature set.

During classification each feature vector is attributed to a class. The primary question being which classificator to opt for as the following are taken under consideration: *Statistically optimal classificators* with the presumption of a probability density of features (Bayes Classification, special forms of Maximum Likelihood Classification), *Classification by means of neuronal nets*, *Support Vector Machine (SVM)*[4],*Minimum Distance Classification.*

The basic principle of classification is depicted in Fig. 15 where a two dimensional feature vector (feature space respectively) ξ is assumed which conduces as base for the object classification. Class I and class II form convex feature vector sets, where the feature vectors ξ usually satisfy a Gaussian distribution with respect to the center of the class. Here the statistical parameters of the density function are determined during the training of the classificator. Considering classes III and IV, the difficulty exists in the fact that the relative frequency is askew, which will, if approximated by Gaussian distribution, definitely produce a wrong classification. In case of minimal or no overlap in the dispersion of the feature space, a classificator which obtains the support space borders of the class by means of non-linear procedures will be applicable (e.g. Support Vector Machine,[4] neuronal nets). In case of overlapping feature vector spaces of different object classes the problem is amplified. Two principal possibilities exist: *adding new features* which step up the dimension of the feature space and thus obtaining a clearer distinction between the classes in question in the new dimensions or *assuming or identifying* the relative frequency of occurrence of the classes. If the relative frequency of one of the overlapping classes is slight, the overall percentage of correct classifications can be increased by accepting occasional wrong classification concerning the smaller class.

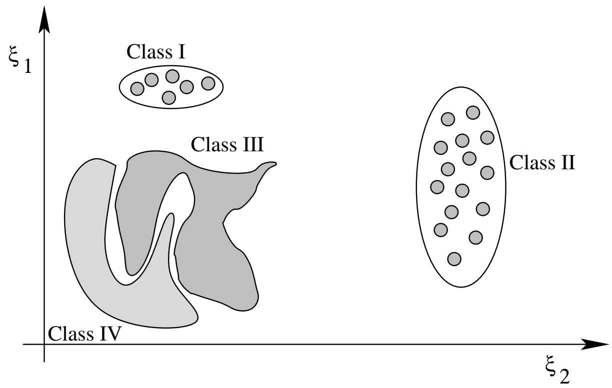

Figure 15: Classification difficulty

In any case the extracted features play a major role in classification. Are those amiss in the separability of the classes, the best classificators are powerless to present a correct and reliable classification, while on the other hand a classificator which is adapted to a certain feature space and the resulting classes can noticeably increase the results in case of non-convex class boundaries.[5]

7. CONCLUSION AND FUTURE WORK

In this paper we have presented our current approach towards the problem of detection of leukemic diseases in medical image processing. Whereas the aim of a fully automated cell analysis and diagnosis of Leukemia (with correct detection rates near 100%) is not yet reached, many important steps in the image acquisition and preprocessing process have been covered. Image acquisition has been standardized and normalized images can be generated. The segmentation based on adaptive thresholding and pixel classification has produced encouraging results although differences is the staining process of the smears can still reduce the rate of segmentation. The declustering has been carried out as described above, the morphological region growing process based on thresholded distance transform is quite robust and yields good results and does not require any startup initialization except for the mask of the cell cluster. The most interesting results are expected in the next phase of the project, when the combination of the intuitive features employed by the physicians and the signal oriented features worked out by image analysts is tested in the setup of a final image analysis system. A set of features is set up and will be tested on a big contingent of pathological and non pathological blood and bone marrow smears.

ACKNOWLEDGMENTS

We thank Prof. Dr. H. Link and Dr. Hagmann from the Westpfalzklinikum for providing image data and extensive support concerning medical issues.

REFERENCES

1. H. Hengen and M. Pandit, "Declustering algorithms for the analysis of blood and bone marrow smears," in *Proceedings of the 2001 SPCOM Conference*, IEEE, (Bangalore), July 2001.
2. J. B. Roerdink and A. Meijster, "The watershed transform: Definition, algorithms and parallelization strategies," *Fundamenta Informaticae (41)* , 2000.
3. A. Hajra, "Segmentation of white blood cells," Master's thesis, Indian Institute of Science, Bangalore, India, 2000.
4. K. Bennett and E. Bredensteiner, "Geometry in learning," in *Geometry at Work*, E. Hart, W. Meyer, and T. Phillips, eds., Mathematical Association of America, Washington D.C., 1997.
5. G. Ongun, U. Halici, K. Leblebicioglu, V. Atalay, M. Beksac, and S. Beksac, "Feature extraction and classification of blood cells for an automated differential blood count system," IEEE, 2001.
6. T. Paulus, "Entwurf und realisierung einer plattform zur akquisition, analyse und segmentierung von mikroskopischen aufnahmen fuer die medizinische bildverarbeitung." Diplomarbeit, 2000.
7. M. Ross, "Methoden der digitalen bildverarbeitung fuer die leukaemiediagnostik." Diplomarbeit, 2000.
8. M. Pandit and H. Hengen, "Image analysis of blood and bone marrow smears," in *Proceedings of the 2001 BIOVISION Conference*, BMESI/IEEE, (Bangalore), December 2001.
9. L. D. Cohen, "On active contur models and balloons," in *Computer Vision, Graphics and Image Processing: Image Understanding*, 1991.